

## One- and two-electron excitations of helium in the $s$ -wave model

M. Draeger, G. Handke, W. Ihra, and H. Friedrich

*Physik Department, Technische Universität München, 85747 Garching, Germany*

(Received 26 April 1994)

The energies of the bound states and energies and widths of autoionizing resonant states of helium are calculated within the  $s$ -wave model, where the individual orbital angular momenta of both electrons are zero. The energies of the bound  $1sns$  states differ from the corresponding energies in real helium only via a small  $n$ -independent shift  $\Delta\mu$  in the quantum defects, which amounts to  $\Delta\mu=0.011$  for singlet states and  $\Delta\mu=0.004$  for triplet states. The quantum defects of more than 50 bound and resonant states with singlet or triplet symmetry are reproduced by an empirical four-parameter formula to within an rms deviation of less than 0.016. The normalized widths of the autoionizing  $Nsns$  resonant states increase with the smaller quantum number  $N$ , and the widths of the singlet states tend to become larger than the separation of successive resonances in the Rydberg series for  $N\approx 8$ . Effects of interference of Rydberg series can be described in the framework of multichannel quantum-defect theory. In the  $7sns$  singlet series of resonances, interference due to the  $8s8s$  perturber inhibits autoionization by more than three powers of 10. Semiclassical quantization based on unstable periodic orbits reproduces the energies of states with equal or similar quantum numbers rather well in a standard application of the cycle-expansion technique and very well in an application using only three nonretracing periodic orbits.

PACS number(s): 31.10.+z, 31.50.+w, 32.80.Dz, 03.65.Sq

### I. INTRODUCTION

Since Madden and Codling's detection of doubly excited states of the helium atom [1] and the first interpretation of their results [2], there has been a continuing interest in two-electron atoms. Despite their seeming simplicity, the correlated motion of two electrons in the Coulomb field of a nucleus is still largely an unsolved problem. There has been considerable experimental [3,4] and theoretical [5–23] progress in recent years, but the energy region just below the two-electron ionization threshold, where many Rydberg series and continua interact, is still only partly understood. Classically the motion of the two electrons in the helium atom is chaotic in large parts of phase space, and two-electron atoms serve as a realistic physical example of chaotic classical dynamics. Substantial progress has recently been made in understanding the classical dynamics in various parts of phase space [15,19,23] and in the semiclassical derivation of quantum-mechanical energy eigenvalues [17,18,22].

Conservation of total linear and total angular momentum reduces the number of independent (spatial) degrees of freedom in two-electron atoms to 4 in the case of nonvanishing total angular momentum, while for vanishing total angular momentum, there are three independent coordinates, e.g., the distances  $r_1, r_2$  of the two electrons from the nucleus and the angle between the corresponding displacement vectors. Simplification of the problem can be achieved within approximative models reduced to two degrees of freedom. Examples are the collinear model, which has been studied in detail in [17–19], and the  $s$ -wave model, which is the subject of the present paper. In this model both electrons are restricted to spherical states,  $r_1$  and  $r_2$  are the only two spatial coordinates, and

all angular correlations are eliminated. Classically this corresponds to two spherical shells of charge  $-1$  expanding and contracting around a fixed nucleus of charge  $Z$ . Comprehensive studies of the classical dynamics of two-electron atoms in the  $s$ -wave model below and above the two-electron ionization threshold have been published in [24–26].

The present paper focuses on the quantum mechanics of  $s$ -wave helium. Several authors have studied electron scattering by hydrogen in the  $s$ -wave model [27–32], but investigations of the spectrum of  $s$ -wave atoms for  $Z > 1$  have so far been restricted to the helium ground state and the lowest triplet state [33–37]. Since the bound states of real helium (below the one-electron ionization threshold) all have  $1snl$  structure—with  $l=0$  for vanishing total angular momentum—the  $s$ -wave model is quite a good approximation of real helium for the bound  $1sns$  states. For the doubly excited states, which all lie above the one-electron ionization threshold and hence are autoionizing resonances, the increasing importance of angular correlations makes a direct comparison of the  $s$ -wave model with real helium less meaningful. Nevertheless, the  $s$ -wave model is perhaps the simplest model for two electrons interacting with each other and with a nucleus via long-ranged Coulomb forces, and interesting features such as the structure of the spectrum below the two-electron ionization threshold and the relation between classical and quantum mechanics are more easily studied in this simple and transparent model. Furthermore, the  $s$ -wave model, where all angular correlations are eliminated, is in a sense complementary to the collinear model, where angular correlations are greatest, so perhaps the behavior of real helium can be expected to lie somewhere in between.

After a brief definition of the  $s$ -wave model in Sec. II, we describe and discuss in Sec. III the results of extensive

numerical calculations of the energies of the bound states and the autoionizing resonant states below the double-ionization threshold. The widths of the resonant states above the one-electron ionization threshold are discussed in Sec. IV. In Sec. V we study the correspondence between the quantum-mechanical spectrum and classical dynamics in the light of modern periodic orbit theory.

## II. *s*-WAVE HELIUM

Assuming infinite nuclear mass, the Hamiltonian of the real helium atom is, in atomic units,

$$H = -\frac{1}{2}\nabla_1^2 - \frac{1}{2}\nabla_2^2 - \frac{Z}{r_1} - \frac{Z}{r_2} + \frac{1}{|\mathbf{r}_1 - \mathbf{r}_2|}. \quad (1)$$

In the subspace defined by individual angular momentum zero of both electrons, the interaction potential

$$\frac{1}{|\mathbf{r}_1 - \mathbf{r}_2|} = \sum_{l=0}^{\infty} \frac{r_{<}^l}{r_{>}^{l+1}} P_l(\cos\theta) \quad (2)$$

contributes only the first term in the sum, and the Hamiltonian of *s*-wave helium is

$$\begin{aligned} H_s &= -\frac{1}{2} \frac{\partial^2}{\partial r_{<}^2} - \frac{Z}{r_{<}} - \frac{1}{2} \frac{\partial^2}{\partial r_{>}^2} - \frac{(Z-1)}{r_{>}} \\ &= H_1 + H_2 + \frac{1}{r_{>}}, \end{aligned} \quad (3)$$

where

$$H_1 = -\frac{1}{2} \frac{\partial^2}{\partial r_1^2} - \frac{Z}{r_1}, \quad H_2 = -\frac{1}{2} \frac{\partial^2}{\partial r_2^2} - \frac{Z}{r_2}. \quad (4)$$

In (3),  $r_{>}$  and  $r_{<}$  denote the larger and the smaller of the two radii  $r_1$  and  $r_2$ , respectively.

As long as  $r_1 > r_2$  or  $r_1 < r_2$ , the electrons move without any coupling potential. The inner electron sees the naked nuclear charge  $Z$  and the outer electron sees a screened charge  $Z-1$ . The Schrödinger equation

$$H_s \Psi(r_1, r_2) = E \Psi(r_1, r_2) \quad (5)$$

is separable in these regions, but coupling is introduced by the requirement of continuous matching at the boundary  $r_1 = r_2$ .

## III. ENERGIES

Below the double-ionization threshold  $E=0$ , the spectrum of helium consists of Rydberg series converging to the limits  $E_N = -Z^2/(2N^2)$ , ( $Z=2$ ). In *s*-wave helium there is, for a given symmetry with respect to exchange of  $r_1$  and  $r_2$ , just one Rydberg series converging to each limit. Each series is associated with a channel defined by a hydrogenic bound-state wave function  $\phi_N$  for one electron, and the contribution of this channel to the total wave function approaches  $\phi_N$  times a highly excited or continuum wave function for the second electron as the energy approaches or exceeds the series limit. The structure of the total wave function is, for  $E < 0$ ,

$$\Psi(r_1, r_2) = \mathcal{A} \sum_{N=1}^{N_0} \phi_N(r_1) \psi_N(r_2) + \mathcal{A} \Phi_b(r_1, r_2), \quad (6)$$

where the sum  $N=1, \dots, N_0$  covers all open channels;  $\phi_N$  stands for the bound hydrogenic function defining the channel  $N$ ;  $\psi_N$  is the generally unbound channel wave function in the open channel  $N$ ; and  $\Phi_b$  is a bound wave function containing no contributions from the open channels. The operator  $\mathcal{A}$  defined by

$$\mathcal{A} \psi(r_1, r_2) = [\psi(r_1, r_2) \pm \psi(r_2, r_1)] / \sqrt{2}$$

ensures the correct spatial symmetry or antisymmetry of the wave function for the singlet and the triplet case, respectively.

For energies below the lowest series limit  $E_1 = -2$ , all channels are closed and the bound states of the system can be obtained by diagonalizing the Hamiltonian (3) in a suitable basis. We chose the basis functions to be products  $\varphi_k(r_1) \varphi_l(r_2)$  of (normalized) Slater-type orbitals:

$$\varphi_k(r) \propto r \exp(-r/a_k). \quad (7)$$

This basis can be made sufficiently dense in Hilbert space if the length parameters are chosen so that the overlap integral between neighboring functions,  $\langle \varphi_k(r) | \varphi_{k\pm 1}(r) \rangle$  is a constant near to 1. We used up to 25 single-electron functions (that is, 625 product wave functions for the two electrons) with an overlap of 0.98 between two neighboring single-electron functions. If the diagonalization is carried out in a basis of no specified symmetry, both singlet and triplet states are calculated simultaneously. We found that an explicit symmetrization or antisymmetrization of the basis does not improve the accuracy of the calculations.

Up to now, the only energy eigenvalues available for *s*-wave helium were those calculated by Winter, Laferrière, and McKoy [35] for the  $1s1s$  ground state ( $-2.879\,035\,0$  a.u.) and for the  $1s2s(^3S)$  excited state ( $-2.174\,254\,68$  a.u.). Our results for the  $1sns$  series are shown in Tables I (singlet) and II (triplet). Our value for the ground-state energy lies less than  $10^{-5}$  a.u. above Winter, Laferrière, and McKoy's result, which was obtained via extrapolation in a calculation optimized for this state. Our lowest triplet state is already an improvement of more than  $10^{-5}$  a.u. over Winter, Laferrière, and McKoy's result. In Table I and II we also show values obtained for the energies of the  $1sns$  bound states of real helium by Bürgers and Wintgen [38] for the singlet states and by Accad, Pekeris, and Schiff [39] for the triplet states. The energies in real helium lie marginally lower than in *s*-wave helium, because angular correlations allow a lowering of the electron-electron repulsion.

An unperturbed Rydberg series of energies  $E_n$  converging to the series limit  $E_N$  can be written in terms of effective quantum numbers  $\nu_n = n - \mu_n$  with slowly varying quantum defects  $\mu_n$  as

$$E_n = E_N - \frac{1}{2\nu_n^2} = E_N - \frac{1}{2(n - \mu_n)^2}. \quad (8)$$

The quantum defects  $\mu_n$  of the  $1sns$  singlet and triplet en-

TABLE I. Energies  $E_n$  and quantum defects  $\mu_n$  of the  $^1S_0$  bound states of  $s$ -wave helium together with the corresponding results of Bürgers and Wintgen [38] for the real three-dimensional helium. The numbers in parentheses are not accurate to all digits quoted—see text.

Configuration ( $^1S_0$ )	$s$ -wave helium		Real helium [38]	
	Energy (a.u.)	Quantum defect	Energy (a.u.)	Quantum defect
1s1s	-2.879 027 69	0.245 80	-2.903 724 377 034 118 9	0.256 18
1s2s	-2.144 188 10	0.137 83	-2.145 974 046 054 35	0.149 25
1s3s	-2.060 788 24	0.132 03	-2.061 271 989 70	0.143 37
1s4s	-2.033 391 81	0.130 41	-2.033 586 716 86	0.141 65
1s5s	-2.021 079 23	0.129 68	-2.021 176 851 15	0.140 92
1s6s	-2.014 507 40	0.129 30	-2.014 563 097 4	0.140 53
1s7s	-2.010 590 97	0.129 04	-2.010 625 775 2	0.140 31
1s8s	-2.008 069 72	0.128 53	-2.008 093 619 1	0.140 16
1s9s	(-2.006 349 35)	(0.125 98)	-2.006 369 551 1	0.140 06
1s10s	(-2.005 119 85)	(0.117 74)	-2.005 142 987 4	0.139 99
1s $\infty$ s	-2.0	0.128	-2.0	0.139 <sup>a</sup>

<sup>a</sup>Reference [43].

ergies converging to the series limit  $E_1 = -2$  are included in Tables I and II for both the  $s$ -wave model and for real helium. The effective quantum numbers in  $s$ -wave helium are a little larger and the quantum defects correspondingly a little smaller than in real helium. This small difference in quantum defects is virtually independent of  $n$  and amounts to  $\Delta\mu = 0.011$  for the singlet states and to  $\Delta\mu = 0.004$  for the triplet states. The dependence of the quantum defects on  $1/v^2 = 2(E_{N=1} - E)$  is displayed in Fig. 1. The fact that the quantum defects begin to drop below the straight lines of convergence near  $n = 10$  indicates that the subspace in which the Hamiltonian was diagonalized is starting to get too small to accurately describe such highly excited states; the energies tend to be too large corresponding to quantum defects which are too small. Extrapolation of quantum defects from the region of obvious convergence yields more accurate energy values for these and higher states. Note that if the quantum defect of a state is known to an accuracy  $\delta\mu$ , then the corresponding energy (8) is accurate to  $\delta\mu/v_n^3 = \delta\mu/(n - \mu_n)^3$ .

The  $1sns$  states are the only exactly bound states. All other states lie above the ionization threshold  $E_1 = -2$  and are hence autoionizing resonances. In this energy region the Schrödinger equation should in principle be

solved with unbound waves in the open channels, e.g., on the basis of the coupled-channel equations. However, the autoionization widths of the states above the ionization threshold are very small, as long as at least one of the two quantum numbers is small, and hence it is a fair approximation to calculate the energies of these states by identifying them with bound states obtained by diagonalizing the Hamiltonian (3) in a subspace orthogonal to the open channels.

Consider a range of energies  $E$  at which the channels  $N = 1, \dots, N_0$  are open, and all other channels are closed, i.e.,

$$-2/N_0^2 < E < -2/(N_0 + 1)^2.$$

Let  $Q$  be the operator projecting onto the space orthogonal to the open channels, i.e., for any single-particle function  $\psi$ ,

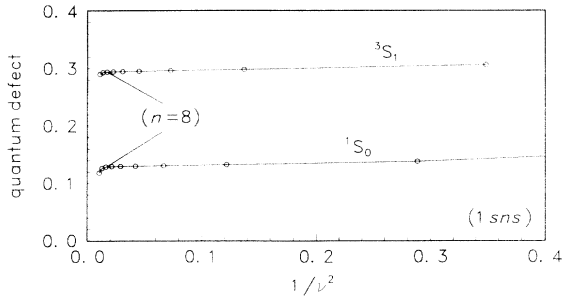
$$\begin{aligned} \langle \phi_N(r_1)\psi(r_2) | Q | \Psi(r_1, r_2) \rangle \\ = \langle \psi(r_1)\phi_N(r_2) | Q | \Psi(r_1, r_2) \rangle = 0 \quad \text{for } 1 < N \leq N_0. \end{aligned} \quad (9)$$

If we expand the total wave function  $\Psi$  in a complete or-

TABLE II. Energies  $E_n$  and quantum defects  $\mu_n$  of the  $^3S_1$  bound state of  $s$ -wave helium together with the results of Accad, Pekris, and Schiff [39] for the real helium.

Configuration ( $^3S_1$ )	$s$ -wave helium		Real helium [39]	
	Energy (a.u.)	Quantum defect	Energy (a.u.)	Quantum defect
1s2s	-2.174 264 80	0.306 13	-2.175 229 378	0.310 80
1s3s	-2.068 490 12	0.298 09	-2.068 689 06	0.302 00
1s4s	-2.036 438 58	0.295 72	-2.036 512 1	0.299 45
1s5s	-2.022 583 64	0.294 69	-2.022 619	0.298 37
1s6s	-2.015 357 90	0.294 17	-2.015 377 5	0.297 80
1s7s	-2.011 117 94	0.293 86	-2.011 129 9	0.297 47
1s8s	-2.008 419 11	0.293 59	-2.008 427 1	0.297 26
1s9s	(-2.006 595 03)	(0.292 84)	-2.006 601 5	0.297 1
1s10s	(-2.005 302 38)	(0.289 32)	-2.005 310 8	0.297 0
1s $\infty$ s	-2.0	0.293	-2.0	0.297 <sup>a</sup>

<sup>a</sup>Reference [43].

FIG. 1. Quantum defects of the  $1sns$  states.

thogonal basis of product wave functions  $\psi_{N_1}(r_1)\psi_{N_2}(r_2)$  and choose the first  $N_0$  basis functions to coincide with the hydrogenic bound-state wave functions  $\phi_N$  defining the open channels, then applying  $Q$  amounts to excluding those terms in the expansion for which  $N_1 \leq N_0$  or  $N_2 \leq N_0$ . For an arbitrary choice of the  $\psi_N$ , applying  $Q$  amounts to orthogonalizing all single-particle wave functions to the hydrogenic wave functions  $\phi_N$ ,  $N=1, \dots, N_0$ , defining the open channels.

Diagonalizing the Hamiltonian  $H_s$  in the space orthogonal to the channels  $N=1, \dots, N_0$  amounts to diagonalizing the Hamiltonian  $QH_sQ$ , which has only bound states for  $E < -2/(N_0+1)^2$ . A considerable simplification can be achieved by applying an idea introduced by Saito [40,41] in the so-called *orthogonality condition model* in nuclear scattering. If we solve the eigenvalue equation for the (non-Hermitian) operator  $QH_s$ ,

$$QH_s\Psi(r_1, r_2) = E\Psi(r_1, r_2), \quad (10)$$

then the eigenfunctions  $\Psi$  automatically fulfill the "orthogonality condition"  $(1-Q)\Psi=0$  as long as  $E \neq 0$ . This follows immediately by applying  $(1-Q)$  to both sides of (10):

$$(1-Q)QH_s\Psi(r_1, r_2) = 0 = E(1-Q)\Psi(r_1, r_2). \quad (11)$$

Hence we only need to solve the eigenvalue problem for  $QH_s$ , as long as we exclude the eigenvalue  $E=0$ . We thus diagonalized  $QH_s$  in the basis defined by the single-particle wave functions (7). The operator  $QH_s$  is invariant under permutation of the two particle labels and its diagonalization automatically yields the symmetric (singlet) and antisymmetric (triplet) eigenstates. The resulting energies and associated quantum defects for the Rydberg series  $Nsns$  with  $N=2, \dots, 9$  are listed in Tables III and IV for singlet and triplet symmetry, respectively.

When the lowest state of the  $(N+1)sns$  series lies below the limit  $E_N = -2/N^2$  of the  $Nsns$  series, it loses its identity as an individual state and becomes instead a perturber of the Rydberg series of states converging to the limit  $E_N$ . This happens first for  $N=5$  in the singlet spectrum where the "6s6s" state lies just below the series limit  $E_5 = -0.08$ . In our present method of diagonalizing the Hamiltonian  $H_s$  in the subspace orthogonal to the "open" channels  $N'=1, \dots, 5$ , we obtain an energy for a 6s6s state lying below  $E_5$  where the channel  $N'=5$  is ac-

tually closed. This energy is not really the energy of an individual state, but corresponds to the position of the perturber of the  $5sns$  series. Similar considerations apply to the  $7s7s$ ,  $8s8s$ ,  $9s9s$ , and  $9s10s$  singlet states. In the triplet spectrum the first case of a state appearing below the series limit of the Rydberg series of the preceding channel occurs when the  $8s9s$  state perturbs the  $7sns$  series converging to  $E_7 = -\frac{2}{49} \approx -0.4082$ . Such fictitious states, which are actually perturbers, are marked by asterisks in the Tables.

The presence of a perturber in a Rydberg series manifests itself in a pseudoresonant jump of the quantum defects of the individual states by unity in analogy to the jump by  $\pi$  of the phase shift near a resonance [42]. For an isolated perturber the quantum defects  $\mu_n$  lie approximately on a curve  $\mu(E)$  given by

$$\mu(E) = \mu_{bg} - \frac{1}{\pi} \arctan \left[ \frac{\Gamma/2}{E - E_R} \right], \quad (12)$$

where  $\mu_{bg}$  is a smoothly varying background term and the arctan term describes the effect of the perturber located at energy  $E_R$  with width  $\Gamma$ .

The quantum defects for the  $Nsns$  series with  $N=5, 6$ , and  $7$  are displayed in Fig. 2 as functions of  $1/v_N^2 = 2(E_N - E)$ . The effect of the lowest state of the next series, viz., the  $(N+1)s(N+1)s$  state perturbing the series, causes the quantum defects of the singlet series to increase towards the series limit, before numerical inaccuracy leads to decreasing values. The 6s6s state perturbing the  $5sns$  series lies close to the limit of the series at high quantum numbers  $n$  out of the range of the present calculation. The perturbation of the  $6sns$  and the  $7sns$  singlet series due to the  $7s7s$  and the  $8s8s$  perturber, respectively, is obvious. A best fit of the quantum defects of the perturbed states to Eq. (12) is obtained for  $E_R = -0.059$  and  $\Gamma = 0.0023$  in the  $6sns$  series and for  $E_R = -0.045$  and  $\Gamma = 0.0016$  in the  $7sns$  series. The energies  $E_R$  obtained in this way agree within the accuracy of the fits with the energies of the (fictitious) states obtained by diagonalizing the Hamiltonian in the space orthogonal to the  $N=6$  or  $7$  states ( $*7s7s$  and  $*8s8s$  in Table III).

There have been a number of attempts to describe the spectra of two-electron atoms by a double Rydberg formula [3,5-7,12-14]. A natural choice, which should work quite well for the spherical electrons of  $s$ -wave helium, is

$$E_{N,n} = -\frac{Z^2}{2N^2} - \frac{(Z-1)^2}{2[n - \mu(N,n)]^2}. \quad (13)$$

For  $n > N$  the outer electron sees a total charge  $Z=1$  due to screening by the inner electron, and the quantum defects  $\mu(N,n)$  converge to an  $n$ -independent constant for  $n \rightarrow \infty$ . The quantum defects depend essentially on the quantum number  $N$  of the inner electron and are virtually independent of  $n$  as long as  $n > N$  or  $n > N+1$  for the singlet and triplet states, respectively.

Clearly the symmetrically excited states  $n=N$  play a special role. If we picture both electrons as moving independently in the Coulomb potential of the nuclear charge partially screened by the other electron, this leads

to the modified Rydberg formula for the total energy:

$$E_{N,N} = -\frac{(Z^*)^2}{(N-\mu_s)^2}. \quad (14)$$

With the  $N$ -independent constants  $(Z^*)^2=2.902\,26$  and  $\mu_s=-0.004\,027$ , Eq. (14) reproduces the energies of the  $NsNs$  singlet states with an accuracy of roughly  $2 \times 10^{-4}$  a.u. or better.

If we force the energies  $E_{N,N}$  from (14) into the form (13), we obtain an explicit expression for the quantum defects  $\mu(N,N)$ , namely,

$$\mu(N,N) = 0.2556N - 0.0096 - \frac{0.0001}{N} + O\left(\frac{1}{N^2}\right). \quad (15)$$

In general, the quantum defects  $\mu(N,n)$  increase with increasing quantum number  $N$  of the inner electron, because its rms radius and its effect of modifying the potential seen by the outer electron increases with  $N$ . If we exclude the  $NsNs$  singlet states and the  $Ns(N+1)s$  triplet states, then a simple linear ansatz,  $\mu = aN + b$  with no dependence on  $n$ , already gives a very good fit to our calculated quantum defects. The deviations of the quantum defects of the lowest states in each series from this simple behavior can be accounted for by adding an empirical term as in the following formulas:

TABLE III. Energies  $E_n$  and quantum defects  $\mu_n$  (modulo unity) of the  $Nsns(^1S_0)$  resonances with  $N=2-9$ . The asterisks mark fictitious states, which are actually perturbers of the Rydberg series of states converging to the limit  $E_{N-1}$ .

Configuration ( $^1S_0$ )	Energy (a.u.)	$\mu_n$	Configuration ( $^1S_0$ )	Energy (a.u.)	$\mu_n$
2s2s	-0.722 650 81	0.501 44	*6s6s	-0.080 549 70	0.527 34
2s3s	-0.571 881 95	0.362 61	6s7s	-0.070 892 52	0.290 27
2s4s	-0.537 615 40	0.354 12	6s8s	-0.066 603 86	0.272 76
2s5s	-0.523 141 73	0.351 78	6s9s	-0.063 968 12	0.290 60
2s6s	-0.515 667 37	0.350 80	6s10s	-0.062 205 68	0.328 98
2s7s	-0.511 307 48	0.350 30	6s11s	-0.060 976 42	0.396 03
2s8s	-0.508 543 59	0.349 94	6s12s	-0.060 096 10	0.506 24
2s9s	-0.506 681 17	0.349 15	6s13s	(-0.059 419 02)	(0.623 82)
2s10s	(-0.505 365 22)	(0.346 36)	6s14s	(-0.058 886 89)	(0.748 88)
2s $\infty$ s	-0.5	0.348			
3s3s	-0.321 419 57	0.754 90	*7s7s	-0.059 220 97	0.787 80
3s4s	-0.265 182 16	0.588 44	7s8s	-0.052 758 37	0.529 38
3s5s	-0.247 779 31	0.576 87	7s9s	-0.049 733 16	0.511 76
3s6s	-0.239 208 83	0.574 60	7s10s	-0.047 824 63	0.553 47
3s7s	-0.234 331 20	0.574 14	7s11s	-0.046 553 99	0.664 93
3s8s	-0.231 289 42	0.574 11	7s12s	-0.045 711 73	0.893 73
3s9s	-0.229 264 60	0.573 93	7s13s	(-0.045 063 55)	(0.149 93)
3s10s	(-0.227 846 40)	(0.571 22)	7s14s	(-0.044 431 12)	(0.239 03)
3s $\infty$ s	-0.22	0.573			
4s4s	-0.181 243 70	0.018 41	*8s8s	-0.045 368 21	0.048 93
4s5s	-0.153 730 82	0.828 32	8s9s	-0.040 813 40	0.769 32
4s6s	-0.143 598 61	0.815 05	8s10s	-0.038 600 29	0.752 30
4s7s	-0.138 071 00	0.815 13	8s11s	-0.037 198 50	0.831 86
4s8s	-0.134 692 21	0.817 53	8s12s	-0.036 316 21	0.065 56
4s9s	-0.132 471 50	0.819 48	8s13s	-0.035 670 99	0.306 32
4s10s	-0.130 928 82	0.816 66	8s14s	(-0.034 993 47)	(0.442 93)
4s11s	(-0.129 799 03)	(0.792 76)			
5s5s	-0.115 921 21	0.269 14	*9s9s	-0.035 850 25	0.306 17
5s6s	-0.100 443 06	0.054 48	*9s10s	-0.032 509 29	0.002 78
5s7s	-0.094 068 02	0.038 32	9s11s	-0.030 840 97	0.983 02
5s8s	-0.090 333 17	0.043 86	9s12s	-0.029 794 41	0.101 49
5s9s	-0.087 921 35	0.055 16	9s13s	-0.029 138 32	0.396 40
5s10s	-0.086 264 99	0.066 43	9s14s	(-0.028 525 89)	(0.580 98)
5s11s	-0.085 071 00	0.070 25			
5s12s	(-0.084 179 95)	(0.062 97)			

$$\mu(N, n) = \begin{cases} 0.2331N - 0.1178 + \frac{0.0051\sqrt{N}}{(n-N)^3 + 0.050} & (16) \\ \text{for singlet states} \\ 0.2444N + 0.2828 + \frac{0.2179\sqrt{N}}{(n-N)^3 + 2.768} & (17) \\ \text{for triplet states.} \end{cases}$$

The  $(n-N)^3$  term in the denominator suppresses the correction for  $n > N$  in the singlet case and for  $n > N + 1$  in the triplet case and thus does not destroy the good fit of the linear ansatz for higher states.

The empirical formulas (16) and (17) are of course only expected to work well in unperturbed Rydberg series. Effects of interchannel perturbations should be described within the framework of multichannel quantum-defect theory, or, more simply, by a formula like (12). On the other hand, the nature of unperturbed  $Nsns$  resonances

coupled mainly to the open channel ( $N-1$ ) is closely related to the nature of a possible low  $NsNs$  or  $Ns(N+1)s$  perturber below the series limit of the  $(N-1)sns$  series. Hence the energies and associated quantum defects of the fictitious states labeled by asterisks in Tables III and IV can be expected to fit into the general behavior described by Eqs. (16) and (17). The four parameters in Eq. (16) were determined by fitting to the quantum defects of the  $Nsns$  singlet states with  $N=1, \dots, 9$  and  $n$  running from  $N$  to  $n_{\max}$ , with  $n_{\max}=10$  for  $N \leq 3$ ,  $n_{\max}=11$  for  $N=4$  and 5, and  $n_{\max}=9$  for  $N=6, \dots, 9$ ; the behavior of the quantum defects for larger  $n$  is distorted due to perturbations or the limits of numerical accuracy. The four-parameter formula (16) reproduces the 52 quantum defects involved with an rms deviation of 0.010. Formula (17) reproduces the quantum defects of 55 triplet states (up to  $n_{\max}=10$  for  $N \leq 3$ ,  $n_{\max}=11$  for  $N=4$  and 5, and  $n_{\max}=12$  for  $N \geq 6$ ) to within 0.016. The good agreement between calculated and empirical quantum defects is illustrated in Fig. 3.

TABLE IV. Same as Table III for the  $Nsns(^3S_1)$  resonances with  $N=2-9$ .

Configuration ( $^3S_1$ )	Energy (a.u.)	$\mu_n$	Configuration ( $^3S_1$ )	Energy (a.u.)	$\mu_m$
2s3s	-0.584 854 77	0.572 57	6s7s	-0.073 000 50	0.646 35
2s4s	-0.542 002 74	0.549 78	6s8s	-0.067 614 19	0.560 74
2s5s	-0.525 156 24	0.541 77	6s9s	-0.064 498 32	0.522 63
2s6s	-0.516 759 46	0.537 96	6s10s	-0.062 477 92	0.501 20
2s7s	-0.511 965 85	0.535 82	6s11s	-0.061 079 24	0.485 84
2s8s	-0.508 971 19	0.534 48	6s12s	(-0.060 057 26)	(0.461 08)
2s9s	-0.506 975 05	0.533 36	6s $\infty$ s	-0.055	0.427
2s10s	(-0.505 575 73)	(0.530 35)			
2s $\infty$ s	-0.5	0.530			
3s4s	-0.272 252 33	0.838 67	7s8s	-0.054 329 66	0.917 20
3s5s	-0.250 564 39	0.799 81	7s9s	-0.050 506 01	0.816 60
3s6s	-0.240 605 13	0.784 72	7s10s	-0.048 198 58	0.770 18
4s7s	-0.235 133 64	0.777 03	7s11s	-0.046 647 29	0.739 92
3s8s	-0.231 793 83	0.772 43	7s12s	(-0.045 528 46)	(0.699 08)
3s9s	-0.229 602 01	0.768 80			
3s10s	(-0.228 080 90)	(0.761 85)			
3s $\infty$ s	-0.22	0.758			
4s5s	-0.157 981 47	0.106 41	*8s9s	-0.042 017 74	0.185 68
4s6s	-0.145 418 12	0.051 46	8s10s	-0.039 200 47	0.069 72
4s7s	-0.139 022 70	0.028 70	8s11s	-0.037 440 84	0.013 09
4s8s	-0.135 252 44	0.016 53	8s12s	(-0.036 216 94)	(0.966 78)
4s9s	-0.132 829 15	0.008 51			
4s10s	-0.131 171 85	0.999 28			
4s11s	(-0.129 977 91)	(0.977 84)			
4s $\infty$ s	-0.125	0.982			
5s6s	-0.103 383 58	0.375 88	*9s10s	-0.033 438 69	0.439 56
5s7s	-0.095 418 80	0.305 45	*9s11s	-0.031 305 50	0.305 43
5s8s	-0.091 055 91	0.275 07	9s12s	-0.029 937 32	0.237 24
5s9s	-0.088 342 69	0.258 38			
5s10s	-0.086 525 98	0.246 90			
5s11s	(-0.085 243 23)	(0.234 70)			
5s $\infty$ s	-0.08	0.208			

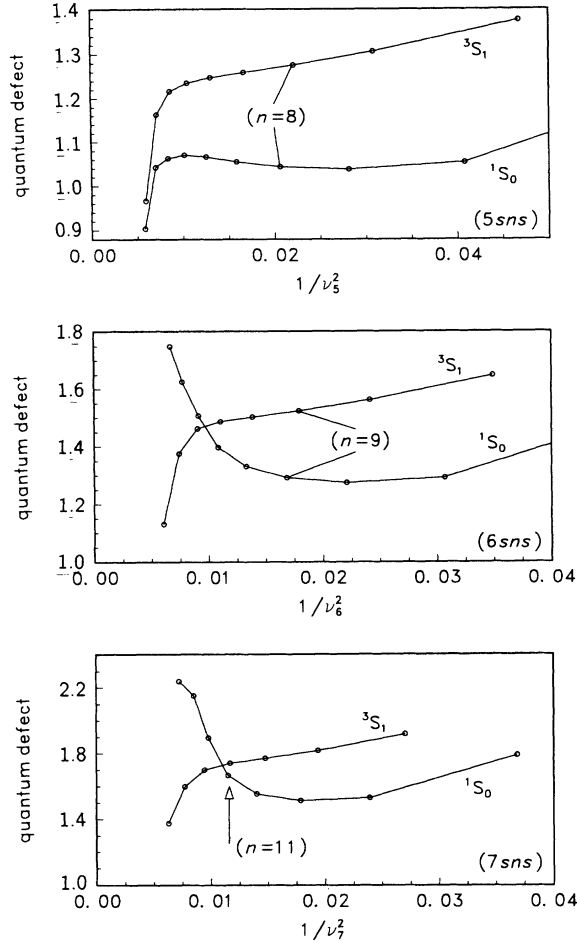


FIG. 2. Quantum defects of the 5sns, 6sns, and 7sns states.

#### IV. LINEWIDTHS

Autoionization widths of an initially bound state  $\Phi_i$  decaying to final states  $\Phi_f$  can be calculated approximately via the "golden rule":

$$\Gamma_{i \rightarrow f} = 2\pi |\langle \Phi_f | H_s | \Phi_i \rangle|^2 \rho(E), \quad (18)$$

which is well justified as long as the total widths are small. In the present case the initial state  $\Phi_i$  is a bound state obtained by diagonalizing  $H_s$  in the space orthogonal to the open channels as described in Sec. III, and the final states  $\Phi_f$  are products of hydrogenic bound states defining an open channel and a continuum wave function for the outgoing electron.

Since a bound-state wave function of a given symmetry in the ket automatically selects the component of the same symmetry in the bra, there is no need to explicitly symmetrize or antisymmetrize the final wave function in the bra. The final wave function in the open channel  $N$ , with energy  $E > E_N = -2/N^2$ , describes the elastic scattering of electron 2 by electron 1, bound in the hydrogenic single-particle state  $\phi_N$ , in the absence of coupling to other channels and has the explicit form

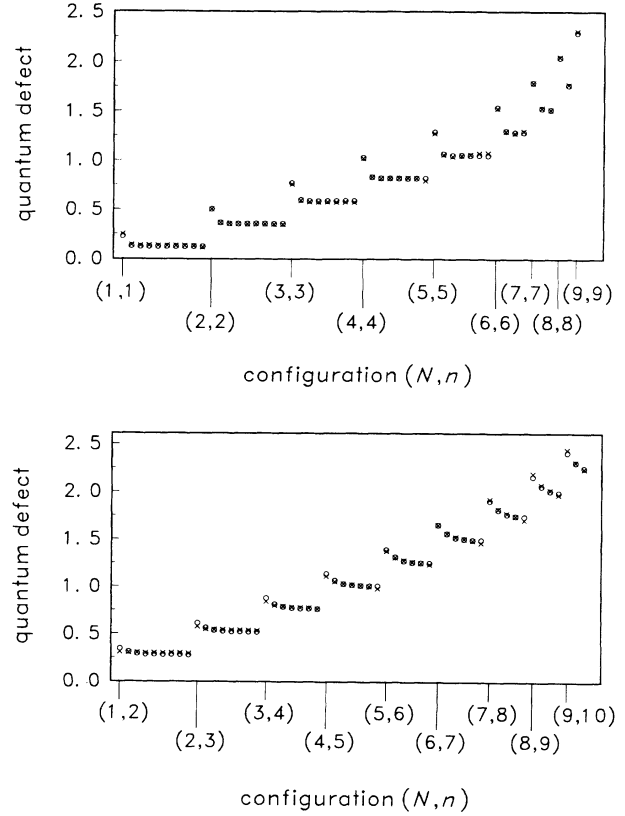


FIG. 3. Quantum defects of the singlet and triplet states as derived from the calculated energies via (13) (X) compared with the values given by the empirical fit (16) and (17) (O). New Rydberg series start at each labeled tick.

$$\Phi_N(r_1, r_2) = \phi_N(r_1) \psi_{\text{reg}}(r_2), \quad (19)$$

where  $\psi_{\text{reg}}(r_2)$  is the regular continuum solution of the uncoupled one-particle Schrödinger equation in channel  $N$ :

$$\left[ H_2 + \int_0^\infty |\phi_N(r_1)|^2 \frac{1}{r_>} dr_1 \right] \psi_{\text{reg}}(r_2) = (E - E_N) \psi_{\text{reg}}(r_2). \quad (20)$$

The wave function (19) is orthogonal to the initial state  $\Phi_i$  and also to  $(H_1 + H_2) \Phi_i$ , where  $H_1$  and  $H_2$  are the single-particle Hamiltonians in Eqs. (3) and (4). This is so because applying  $H_1 + H_2$  to  $\Phi_i$  does not destroy its orthogonality to all open channels. Hence, only the coupling term  $1/r_>$  of the Hamiltonian  $H_s$  contributes to the matrix element in (18). If we choose the asymptotic normalization of the continuum wave functions in (20) such that they are normalized in energy, then the density of final states is unity. With these concretizations the golden rule formula (18) for the decay width by autoionization into the open channel  $N$  becomes

$$\Gamma_i(N) = 2\pi \left| \left\langle \phi_N(r_1) \psi_{\text{reg}}(r_2) \left| \frac{1}{r_>} \right| \Phi_i \right\rangle \right|^2. \quad (21)$$

A more precise calculation of the decay widths involves

solving the coupled-channel equations for the continuum wave functions in the open channels. This can be done without further approximation at energies with a finite number of open channels, if we restrict the bound part of the wave function (6) to lie within a finite-dimensional Hilbert space. For just one open channel the wave function is

$$\Psi(r_1, r_2) = \phi_1(r_1)\psi(r_2) + \sum_{j=1}^n a_j \Phi_j(r_1, r_2). \quad (22)$$

Here  $\phi_1$  denotes the hydrogenic  $1s$  wave function (for  $Z=2$ ),  $\psi$  is a continuum wave function to be determined, and  $\Phi_j$  are the bound-state wave functions obtained by diagonalizing the Hamiltonian in the space orthogonal to the open channel as described in Sec. III. Inserting (22) into the Schrödinger equation, multiplying from the left with  $\phi_1^*(r_1)$ , and integrating over  $r_1$  yields

$$\left[ (E - E_1) - \left[ H_2 + \int_0^\infty |\phi_1(r_1)|^2 \frac{1}{r_>} dr_1 \right] \right] \psi(r_2) = \sum_{j=1}^n a_j \langle \phi_1 | H_s | \Phi_j \rangle_{r_1}, \quad (23)$$

where the subscript  $r_1$  on the matrix element means integration over  $r_1$  only. Multiplying the Schrödinger equation from the left with a bound state  $\Phi_k^*$  and integrating over  $r_1$  and  $r_2$  yields

$$(E - E_k) a_k = \langle \Phi_k | H_s | \phi_1(r_1)\psi(r_2) \rangle = \langle \Phi_k | 1/r_> | \phi_1(r_1)\psi(r_2) \rangle. \quad (24)$$

Note again that only the coupling term  $1/r_>$  contributes to the matrix elements of the Hamiltonian  $H_s$  between open-channel wave functions and the bound states  $\Phi_k$  (which are orthogonal to all open channels).

In the absence of channel coupling, Eq. (23) reduces to the homogeneous equation (20) with the regular (energy-normalized) solution  $\psi_{\text{reg}}(r_2)$  and a corresponding irregular solution  $\psi_{\text{irr}}(r_2)$ , which asymptotically differs from  $\psi_{\text{reg}}$  only in a phase shift of  $\pi/2$ . The Green's function of this homogeneous equation is [42]

$$G(r_2, r'_2) = -\pi \begin{cases} \psi_{\text{reg}}(r'_2)\psi_{\text{irr}}(r_2) & \text{for } r_2 \geq r'_2 \\ \psi_{\text{reg}}(r_2)\psi_{\text{irr}}(r'_2) & \text{for } r'_2 \geq r_2. \end{cases} \quad (25)$$

This Green's function can be used to formally solve the inhomogeneous equation (23),

$$\psi(r_2) = \psi_{\text{reg}}(r_2) + \sum_{j=1}^N a_j G_j(r_2), \quad (26)$$

where the abbreviation  $G_j(r_2)$  is used for the following double integral:

$$G_j(r_2) = \int_0^\infty G(r_2, r'_2) \left[ \int_0^\infty \phi_1^*(r_1)(r_>)^{-1} \times \Phi_j(r_1, r'_2) dr_1 \right] dr'_2. \quad (27)$$

Asymptotically ( $r_2 \rightarrow \infty$ ), we can assume  $r_2 \geq r'_2$ , and (26) becomes

$$\psi(r_2) = \psi_{\text{reg}}(r_2) - \pi \psi_{\text{irr}}(r_2) \sum_{j=1}^N a_j \langle \phi_1 \psi_{\text{reg}} | (r_>)^{-1} | \Phi_j \rangle. \quad (28)$$

Inserting (26) into (24) gives an inhomogeneous system of  $N$  linear equations for the  $N$  coefficients  $a_j$ :

$$(E - E_k) a_k = \langle \Phi_k | (r_>)^{-1} | \phi_1(r_1)\psi_{\text{reg}}(r_2) \rangle + \sum_{j=1}^N \langle \Phi_k | (r_>)^{-1} | \phi_1(r_1)G_j(r_2) \rangle a_j. \quad (29)$$

With the coefficients  $a_j$  obtained by solving (29), Eq. (28) is an explicit solution for the asymptotic open-channel wave function, and the quotient of the coefficients of the irregular and regular solutions of the homogeneous equation is the tangent of the phase shift due to coupling to the bound states  $\Phi_j$ :

$$\tan \delta(E) = -\pi \sum_{j=1}^N \langle \phi_1 \psi_{\text{reg}} | (r_>)^{-1} | \Phi_j \rangle a_j. \quad (30)$$

This result corresponds to the exact solution of the Schrödinger equation in the space spanned by all wave functions of the form (22) and involves no further approximations.

Once the energy dependence of the phase shifts (30) is known, the resonance energies  $E_R$  can be identified as points of maximum gradient  $d\delta/dE$  and the resonance

TABLE V. The widths of the  $2sns$  resonances. Method 1 is based on a full solution of the coupled-channel equations, method 2 on the golden rule. The exponents (base 10) are in brackets. The last column shows the normalized widths  $\Gamma_{2n}^* = (n - \mu_n)^3 \Gamma_{2n}$ .

Configuration ( $1S_0$ )	Method 1,	Method 2	
	Width $\Gamma_{2n}$ (a.u.)	Width $\Gamma_{2n}$ (a.u.)	Normalized width $\Gamma_{2n}^*$ (a.u.)
$2s2s$	4.400 [-4]	4.802 [-4]	1.616 [-3]
$2s3s$	9.855 [-5]	1.063 [-4]	1.950 [-3]
$2s4s$	4.046 [-5]	4.289 [-5]	2.079 [-3]
$2s5s$	2.034 [-5]	2.116 [-5]	2.125 [-3]
$2s6s$	1.136 [-5]	1.191 [-5]	2.147 [-3]
$2s7s$	6.990 [-6]	7.355 [-6]	2.163 [-3]
$2s8s$		4.854 [-6]	2.173 [-3]
$2s9s$		3.389 [-6]	2.194 [-3]

TABLE VI. Partial and total widths of the  $Nsns(^1S_0)$  resonances for  $N=3-5$ .  $\Gamma_{Nn}^*(N')$  stands for the partial width for decay into channel  $N'$ , normalized in analogy to (32) by multiplication with the cube  $(n - \mu_n)^3$  of the effective quantum number in the Rydberg series.  $\Gamma_{Nn}^*$  is the total normalized width and  $\Gamma_{Nn}$  is the actual autoionization width without the normalizing factor.

Configuration ( $^1S_0$ )	Total width $\Gamma_{Nn}$ (a.u.)	Normalized total width $\Gamma_{Nn}^*$ (a.u.)	Partial widths (a.u.)		
			$\Gamma_{Nn}^*(N-1)$	$\Gamma_{Nn}^*(N-2)$	$\Gamma_{Nn}^*(N-3)$
3s3s	1.167 [-3]	1.321 [-2]	1.294 [-2]	2.662 [-4]	
3s4s	3.293 [-4]	1.308 [-2]	1.271 [-2]	3.629 [-4]	
3s5s	1.581 [-4]	1.368 [-2]	1.326 [-2]	4.130 [-4]	
3s6s	8.665 [-5]	1.384 [-2]	1.340 [-2]	4.346 [-4]	
3s7s	5.230 [-5]	1.388 [-2]	1.343 [-2]	4.453 [-4]	
3s8s	3.387 [-5]	1.387 [-2]	1.342 [-2]	4.512 [-4]	
3s9s	2.312 [-5]	1.383 [-2]	1.338 [-2]	4.540 [-4]	
3s10s	1.630 [-5]	1.366 [-2]	1.321 [-2]	4.509 [-4]	
4s4s	5.318 [-4]	1.410 [-2]	1.372 [-2]	3.533 [-4]	2.833 [-5]
4s5s	1.287 [-4]	9.341 [-3]	9.061 [-3]	2.451 [-4]	2.451 [-5]
4s6s	6.277 [-5]	8.749 [-3]	8.526 [-3]	1.832 [-4]	3.937 [-5]
4s7s	3.497 [-5]	8.273 [-3]	8.087 [-3]	1.450 [-4]	4.076 [-5]
4s8s	2.143 [-5]	7.941 [-3]	7.781 [-3]	1.190 [-4]	4.105 [-5]
4s9s	1.415 [-5]	7.748 [-3]	7.610 [-3]	9.700 [-5]	4.081 [-5]
4s10s	1.001 [-5]	7.749 [-3]	7.637 [-3]	7.117 [-5]	4.021 [-5]
4s11s	1.092 [-5]	1.099 [-2]	1.089 [-2]	4.879 [-5]	5.360 [-5]
5s5s	3.637 [-3]	1.889 [-1]	1.879 [-1]	9.246 [-4]	1.364 [-6]
5s6s	9.262 [-4]	1.120 [-1]	1.111 [-1]	7.421 [-4]	1.214 [-6]
5s7s	5.143 [-4]	1.090 [-1]	1.083 [-1]	6.943 [-4]	5.082 [-6]
5s8s	3.112 [-4]	1.047 [-1]	1.041 [-1]	6.539 [-4]	9.124 [-6]
5s9s	1.985 [-4]	9.952 [-2]	9.889 [-2]	6.081 [-4]	1.345 [-5]
5s10s	1.327 [-4]	9.460 [-2]	9.398 [-2]	5.950 [-4]	2.011 [-5]
5s11s	1.343 [-4]	1.315 [-1]	1.306 [-1]	8.797 [-4]	4.663 [-5]
5s12s	1.050 [-4]	1.373 [-1]	1.362 [-1]	1.028 [-3]	7.616 [-5]
*6s6s	1.379 [-4]	1.234 [-2]		1.223 [-2]	9.823 [-5]
6s7s	1.579 [-3]	2.939 [-1]	2.805 [-1]	1.337 [-2]	5.601 [-5]
6s8s	8.918 [-4]	2.716 [-1]	2.560 [-1]	1.539 [-2]	4.002 [-5]
6s9s	5.476 [-4]	2.509 [-1]	2.353 [-1]	1.559 [-2]	2.885 [-5]
6s10s	3.304 [-4]	2.154 [-1]	2.014 [-1]	1.390 [-2]	2.088 [-5]
6s11s	1.668 [-4]	1.477 [-1]	1.382 [-1]	9.453 [-3]	1.277 [-5]
6s12s	3.301 [-5]	3.814 [-2]	3.606 [-2]	2.067 [-3]	1.238 [-6]
6s13s	1.281 [-5]	1.885 [-2]	1.670 [-2]	2.109 [-3]	1.252 [-5]
6s14s	1.327 [-4]	2.440 [-1]	2.231 [-1]	2.074 [-2]	6.249 [-5]
*7s7s	2.196 [-4]	3.109 [-2]		2.781 [-2]	3.277 [-3]
7s7s	2.3 [-3]	3.3 [-1]			
7s8s	2.740 [-3]	7.422 [-1]	7.094 [-1]	2.875 [-2]	4.038 [-3]
7s9s	1.399 [-3]	5.872 [-1]	5.489 [-1]	3.334 [-2]	5.008 [-3]
7s10s	8.160 [-4]	4.917 [-1]	4.551 [-1]	3.170 [-2]	4.932 [-3]
7s11s	3.230 [-4]	2.628 [-1]	2.431 [-1]	1.699 [-2]	2.678 [-3]
7s12s	3.746 [-7]	3.867 [-4]	2.815 [-4]	8.501 [-5]	1.946 [-5]
7s13s	2.107 [-4]	2.692 [-1]	2.404 [-1]	2.467 [-2]	4.140 [-3]
7s14s	2.573 [-4]	4.187 [-1]	3.764 [-1]	3.617 [-2]	6.083 [-3]
*8s8s	2.993 [-4]	6.309 [-2]		5.457 [-2]	7.109 [-3]
8s8s	1.6 [-3]	3.37 [-1]			
8s9s	(7.548 [-2])	(2.854 [+1])	(2.847 [+1])	5.290 [-2]	8.532 [-3]
8s10s	2.216 [-3]	1.243 [+0]	1.169	6.130 [-2]	1.072 [-2]
8s11s	1.086 [-3]	8.370 [-1]	7.753 [-1]	4.976 [-2]	9.053 [-3]
8s12s	9.635 [-5]	9.447 [-2]	8.926 [-2]	4.226 [-3]	7.462 [-4]
8s13s	2.377 [-4]	2.859 [-1]	2.533 [-1]	2.584 [-2]	5.107 [-3]
8s14s	4.881 [-4]	7.534 [-1]	6.760 [-1]	6.128 [-2]	1.218 [-2]

widths  $\Gamma$  are defined via these maximum gradients:

$$\Gamma = 2 \left[ \frac{d\delta}{dE} \Big|_{E=E_R} \right]^{-1}. \quad (31)$$

Table V shows the widths for decay via autoionization of the  $2sns$  singlet series as calculated via exact diagonalization and application of the formula (31) (method 1) in comparison with the results obtained via the golden rule (21). Agreement is good and suggests that the simpler golden rule formula is sufficient to derive accurate values for the widths, at least as long as they are substantially smaller than the separation of successive resonances. The widths of the triplet states are very small and no reliable values could be obtained in the present calculations, so we discuss only the widths of the singlet states in the following.

The partial widths of the  $Nsns$  resonant states with  $3 \leq N \leq 8$ , calculated via the golden rule, are shown in Table VI.  $\Gamma_{Nn}^*(N')$  stands for the partial width for decay into channel  $N'$ , normalized by multiplication with the cube  $(n - \mu_n)^3$  of the effective quantum number in the Rydberg series. In an unperturbed Rydberg series of resonances in channel  $N$  which can decay by autoionization into the open channel  $N'$ , the normalized (partial) decay widths are typically given by [42]

$$\Gamma_{Nn}^*(N') = (n - \mu_n)^3 \Gamma_{Nn} = \frac{2}{\pi} R_{N',N}^2, \quad (32)$$

where  $R_{N',N}$  is an essentially  $n$ -independent parameter describing the coupling between channels  $N$  and  $N'$ . In Table VI,  $\Gamma_{Nn}^*$  is the total normalized width  $\Gamma_{Nn}^* = \sum_{N'} \Gamma_{Nn}^*(N')$ , and  $\Gamma_{Nn}$  is the actual autoionization width without the normalizing factor. Examining the partial widths for decay of a given state  $Nsns$  into various open channels shows that decay into the closest open channel is by far most probable.

The normalized widths of the singlet states in Table VI tend to increase with increasing channel label  $N$  and are

$$\begin{aligned} \Gamma^* &= \nu_N^3 \Gamma \\ &= \frac{2}{\pi} R_{N-1,N}^2 \frac{(T_{N+1} - R_{N,N+1} R_{N-1,N+1} / R_{N-1,N})^2}{T_{N+1}^2 + R_{N,N+1}^4 + (\nu_{N+1} / \nu_N)^3 (T_{N+1}^2 + 1) R_{N,N+1}^2}, \end{aligned} \quad (33)$$

where

$$T_{N+1} = \tan[\pi(\nu_{N+1} + \mu_{N+1})].$$

The parameter  $\mu_{N+1}$  describes the background effect of the deviation of the perturbing channel  $N+1$  from a pure Coulomb problem in the absence of channel coupling,  $\nu_i(E)$  stands for the continuous effective quantum number  $\nu_i = 1/\sqrt{2(E_i - E)}$  in the closed channels  $i = N$  and  $i = N+1$ , and  $R_{i,j} = R_{j,i}$  are real coupling constants describing the coupling between channels  $i$  and  $j$ . Points of vanishing width of resonances or pseudoresonant perturbations occur whenever

$$T_{N+1} = R_{N,N+1} R_{N-1,N+1} / R_{N-1,N}, \quad (34)$$

occasionally larger than unity for  $N = 8$ . This means that the individual widths are larger than the typical separation of successive resonances in the respective Rydberg series, the resonances overlap, and a spectrum of individual lines is replaced by a continuum. The application of the golden rule can no longer be expected to be quantitatively reliable when the resulting widths are so large.

The smallness of the variations of the normalized partial widths in the unperturbed parts of the Rydberg series shows how well the approximate formula (32) is fulfilled. However, the interference of different Rydberg series leads not only to perturbations in the positions of the resonances, but also to dramatic effects on their widths. When a Rydberg series of autoionizing resonances in channel  $N$  is perturbed by resonances from a second series, e.g., in channel  $(N+1)$ , dramatic deviations from simple formulas like (32) occur. In particular, if all resonances can decay into only one and the same open channel, destructive interference can lead to the total vanishing of the widths of certain states in the perturbed series of resonances [44]. This phenomenon, which has been called ‘‘inhibited autoionization’’ [45] or ‘‘stabilization’’ [46], is accurately described by multichannel quantum-defect theory (MQDT) applied for two closed and one open channel [42,47,48].

In the present case there are always several channels open at energies for which interference of resonances occurs, so an exact vanishing of autoionization widths is improbable. However, since the decay of resonances in a given channel  $N$  into the adjacent (open) channel  $(N-1)$  is by far the dominant decay mode, perturbation of this series of resonances by states from the closed channel  $(N+1)$  can lead to very strong inhibition of autoionization and to anomalously stable states above the ionization threshold. Restricting the description to three adjacent channels, viz., the open channel  $(N-1)$ , and the closed channels  $N$  and  $(N+1)$ , the widths  $\Gamma$  of the resonances are given approximately by [47,48]

and stabilization of a resonance occurs when its position lies close to an energy fulfilling (34).

Figure 4 shows the normalized (total) autoionization widths of the  $6sns$  and  $7sns$  singlet series plotted against the continuous effective quantum number  $\nu_{N+1} = 1/\sqrt{2(E_{N+1} - E)}$  of the perturbing channels  $N+1=7$  and  $N+1=8$ , respectively. The solid curves show the results of an MQDT fit including the three channels 5, 6, and 7 and 6, 7, and 8, respectively. The MQDT parameters in the upper part of the Figure are the coupling constants in the second column of Table VII together with the background quantum defect  $\mu_7 = 0.79$ . The MQDT parameters in the lower part of the Figure are the coupling constants in the third column of Table

TABLE VII. Three-channel quantum defect theory parameters for channels 5, 6, and 7 and 6, 7, and 8. The second to last column shows the coupling strengths  $|R_{ij}|$  derived from the partial widths (Table VI) via (32); the last column shows the coupling strengths derived analogously from the widths of the corresponding perturbers derived via (12).

Parameter	3QDT fit (5, 6, and 7)	3QDT fit (6, 7, and 8)	$ R_{ij} $ from decay widths	$ R_{ij} $ from quantum defects
$R_{56}$	-0.63		0.61	
$R_{57}$	-0.20		0.23	
$R_{67}$	-0.53	-0.96	0.84	0.71
$R_{68}$		-0.29	0.29	
$R_{78}$		-0.68	0.88	0.73

VII together with the background quantum defect  $\mu_8=0.05$ . Note that these quantum defects agree with the quantum defects of the respective fictitious states  $^*7s7s$  and  $^*8s8s$  as listed in Table III. The coupling parameters  $R_{i,j}$  obtained in the MQDT fit are also consistent with the partial widths for decay from the closed channels into the open channel  $N-1$ , which approximately follow (32) in the unperturbed part of a Rydberg series of resonances. The fourth column in Table VII

lists the absolute values of the coupling constants as estimated according to (32) from the partial decay widths in Table VI. The fictitious states  $^*7s7s$  and  $^*8s8s$  appear as perturbers of the  $6sns$  series and the  $7sns$  series, respectively, and the widths of these perturbers as derived from the quantum defects of the perturbed series via (12) can also be related to the (dominant) coupling constants  $R_{6,7}$  and  $R_{7,8}$  in analogy to (32). The absolute widths of the coupling constants estimated in this way are included in the last column in Table VII. The entries in different columns of Table VII do not agree exactly, because they are based on different approximations. The qualitative agreement does, however, show that the various approximate MQDT descriptions are consistent with each other and with the results of the full scale calculation.

The perturbation due to the  $7s7s$  state leads to a point of vanishing width near  $\nu_7=5.15$  in the  $6sns$  series of res-

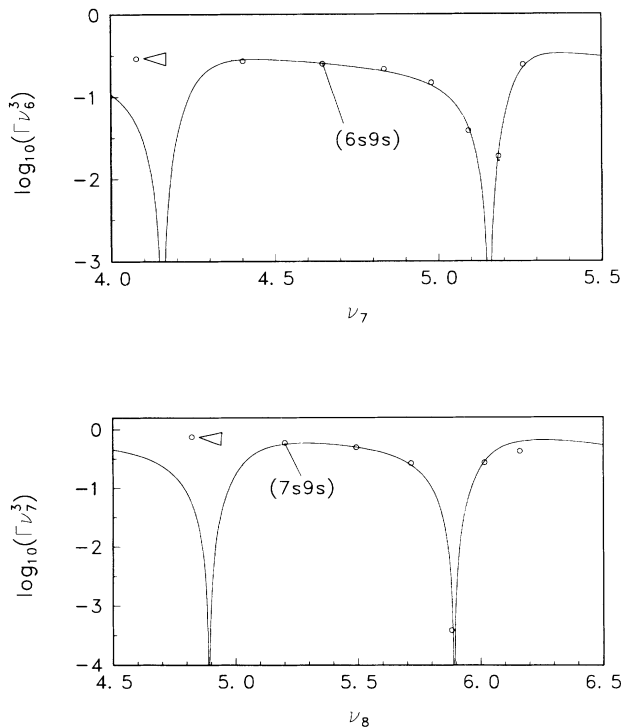


FIG. 4. Autoionization widths for the  $6sns$ -( $^1S_0$ ) series, which is perturbed by the  $7s7s$ ( $^1S_0$ ) state (top) and for the  $7sns$ ( $^1S_0$ ) series perturbed by the  $8s8s$ ( $^1S_0$ ) state (bottom). The open circles show the calculated normalized total autoionization widths and the solid lines show the results of an MQDT fit based on the three channels  $N-1$ ,  $N$ , and  $N+1$  corresponding to 5, 6, and 7 (top) and to 6, 7, and 8 (bottom). The dips in the solid lines at low effective quantum numbers  $\nu_{N+1}$ ,  $\nu_7 \approx 4.3$  (top), and  $\nu_8 \approx 4.9$  (bottom) are artifacts due to the periodicity of the MQDT formulas; in these regions, where there are no perturbers, it is more physical to extrapolate the solid lines smoothly as indicated by the arrows.

TABLE VIII. Properties of periodic orbits of  $s$ -wave helium. The orbits are represented by the corresponding code.  $S$  is the (scaled) action,  $\lambda$  the Lyapunov exponent, and  $\alpha$  the Morse index.  $C$  gives the character of the periodic orbit (h for hyperbolic and ih for inverse hyperbolic).

$s$ -wave helium				
(+, -) code	$S/2\pi$ (a.u.)	$\lambda$	$\alpha$	$C$
-	1.725 58	0.204	2	ih
+-	3.416 59	0.183	4	ih
++-	5.060 31	0.173	6	ih
+--	5.124 71	0.171	6	h
+++	6.665 29	0.165	8	ih
++--	6.742 48	0.154	8	h
+---	6.857 34	0.193	8	ih
++++	8.242 57	0.152	10	ih
+++--	8.326 42	0.139	10	h
++-+-	8.471 79	0.177	10	h
++---	8.485 62	0.187	10	ih
+----	8.547 51	0.181	10	ih
-----	8.580 79	0.191	10	h
+++++	9.799 87	0.142	12	ih
++++-	9.887 72	0.126	12	h
+++--	10.069 35	0.167	12	h
+++---	10.078 52	0.179	12	ih
++-+-	10.175 40	0.174	12	ih
++-+-	10.175 40	0.174	12	ih
+----	10.206 16	0.182	12	h
+----	10.275 16	0.190	12	h
-----	10.307 11	0.195	12	ih

onances (upper part of Fig. 4) and the perturbation due to the  $8s8s$  state leads to a point of vanishing width near  $\nu_8=5.89$  in the  $7sns$  series of resonances (lower part of Fig. 4). The dips in normalized width at lower values of  $\nu_{N+1}$ , viz., near 4.3 and 4.9, respectively, are artifacts due to the periodicity of the MQDT formula (33) in the effective quantum number  $\nu_{N+1}$ ; in these regions, where there are no perturbers, it is more physical to extrapolate the solid lines smoothly as indicated by the arrows. In the present case the widths of the  $6s12s$  and  $6s13s$  states are roughly a factor 10 smaller than would be expected in an unperturbed series of resonances with constant normalized width; in the  $7sns$  series the total autoionization width of the  $7s12s$  state is suppressed by a factor of roughly  $10^{-3}$ .

## V. CLASSICAL-QUANTUM CORRESPONDENCE

The study of the semiclassical behavior of classically chaotic systems is a topic of great current interest, e.g., in connection with the general problem of how chaos manifests itself in quantum mechanics. One access to semiclassical quantization in chaotic systems is provided by Gutzwiller's trace formula, which connects the quantum-mechanical spectrum to a sum over the classical periodic orbits. If the trace of the quantum-mechanical Green's function

$$g(E) = \sum_{j=1}^{\infty} \frac{1}{E - E_j} \quad (35)$$

( $E_j$  are the eigenvalues of the quantum-mechanical Hamiltonian) is calculated in the semiclassical limit, it can be expressed as a sum over the periodic orbits of the corresponding classical system [49]:

$$g_{SC}(E) = \frac{1}{i\hbar} \sum_{PO} T_{PO}(E) \sum_{n=1}^{\infty} \frac{1}{\sqrt{\det(\underline{M}_{PO}^n - \underline{1})}} \times \exp \left[ in \left( \frac{S_{PO}}{\hbar} - \mu_{PO} \frac{\pi}{2} \right) \right]. \quad (36)$$

The first sum runs over all primitive (i.e., nonrepeated) periodic orbits with period  $T_{PO}$ , action  $S_{PO} = \oint \mathbf{p} \cdot d\mathbf{x}$ , and Morse index  $\mu_{PO}$ . The second sum takes into account  $n$ -fold repetitions.  $\underline{M}_{PO}$  is the stability matrix of the respective periodic orbit. The periodic orbits of  $s$ -wave helium are very similar to those of the collinear configuration of the helium atom which have been investigated by Wintgen *et al.* [17,18]. They are all unstable and can be enumerated by a symbolic binary code which registers collisions of the orbits with the  $r_1$  axis and the  $r_2$  axis during one period. Two consecutive collisions with the same axis are coded as “+,” with different axes as “-.” Four examples of periodic orbits of  $s$ -wave helium are shown in Fig. 5. The relevant properties of the periodic orbits of  $s$ -wave helium are summarized in Table VIII for all periodic orbits up to code length 6. For a comprehensive description of the classical dynamics of  $s$ -wave helium, see [24,26].

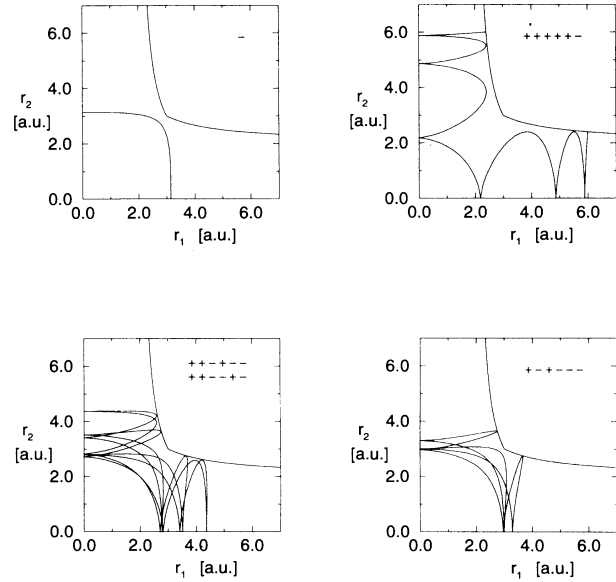


FIG. 5. Four periodic orbits together with their code and the equipotential line at  $-1$  a.u. The orbit “+++++---” grows out of the alternating oscillation “-” by addition of a tail of separable oscillations in the intermittent regions. The orbits “++++--” and “++-----” are the time-reversed images of each other; they and the orbit “++-----” (which is symmetric under time reversal) are the only three nonretracing orbits up to code length 6.

The imaginary part of the trace (35) is essentially the quantum-mechanical level density and hence Gutzwiller's formula (36) expresses the level density in terms of the classical periodic orbits. Long-range correlations in the energy spectrum are largely determined by short periodic orbits with small actions  $S_{PO}$ . In the Fourier transform of the quantum-mechanical spectrum, the long-range correlations of the spectrum become visible as pronounced peaks, which are located at the periods of the short periodic orbits [49]. In the present case the equations of motion can be scaled to energy-independent form and the energy-independent scaled action is  $S^{(s)} = \sqrt{-E}S$ . In terms of the scaled actions the exponentials in (36) have the form  $\exp\{in[(S^{(s)}/\hbar)/\sqrt{-E} - \dots]\}$ . If we regard the spectrum as a function of  $1/\sqrt{|E|}$  and perform a Fourier transform, then the Fourier-transformed spectrum is characterized by peaks located at the scaled actions of the periodic orbits [50]. Figure 6 shows the Fourier transform based on 18 singlet states of  $s$ -wave helium with similar quantum numbers  $n \approx n$ . The actions of the periodic orbits with code length up to 6 are marked with arrows and it can be seen that the positions of the peaks are in good agreement with these actions. Note, however, that the positions of the peaks also agree with multiples of the action of the shortest orbit “-.”

Beyond the usefulness of Gutzwiller's formula in understanding the role of short periodic orbits in chaotic (and other) systems, there is currently keen interest in using this or related formulas to quantitatively derive, in the semiclassical limit, the energies of individual levels of

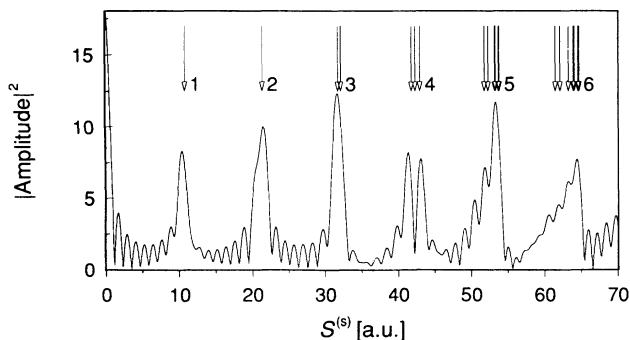


FIG. 6. Fourier-transformed spectrum based on 18 singlet states of  $s$ -wave helium with similar quantum numbers. The arrows mark the actions of the periodic orbits and the numbers beside each group of arrows give the code length.

the spectrum [51]. In a chaotic system the number of (unstable) periodic orbits proliferates exponentially with increasing action of the orbits and the sum in (36) is in no way convergent, at least for real energies  $E$ . Hence a complete summation of the trace formula is impossible and suitable approximations are necessary. Despite the multifarious efforts and some success in special cases [51], there is no established method for evaluation of this formula in a general system.

One popular method of extracting eigenvalues out of the trace formula is based on writing it as an infinite product which has its zeros at the quantum energy eigenvalues [49,52]. In a system with two degrees of freedom and only hyperbolic or inverse hyperbolic orbits, this yields

$$\prod_j (E - E_j) \sim \prod_{\text{PO}} \prod_{k=0}^{\infty} (1 - t_{\text{PO}}^{(k)}), \quad (37)$$

with

$$t_{\text{PO}}^{(k)} = (\pm 1)^k \exp \left[ i \left[ \frac{S_{\text{PO}}}{\hbar} - \mu_{\text{PO}} \frac{\pi}{2} \right] - \left[ k + \frac{1}{2} \right] \lambda_{\text{PO}} T_{\text{PO}} \right]. \quad (38)$$

Here  $\lambda_{\text{PO}}$  stands for the Lyapunov exponent which is a quantitative measure of the instability of a given periodic orbit. The  $+$  sign applies to hyperbolic, the  $-$  sign to inverse hyperbolic orbits. The infinite product (37) is also divergent, and its zeros are not just the zeros of the factors. Various techniques for a numerical evaluation of the product (37) have been proposed in recent years. Usually one expands the product into a sum of terms  $\pm \prod_i t_{\text{PO}_i}^{(k_i)}$  and truncates the sum while arguing, e.g., that the contributions from long periodic orbits are approximately accounted for by combinations of short orbits [53–55]. This is the basis of the so-called cycle expansion which yields good results for the anisotropic Kepler problem [56,57] and for the helium atom on the basis of collinear periodic orbits [17,18], and where all products  $\pm \prod_i t_{\text{PO}_i}^{(k_i)}$  up to a given total code length are included in

the truncated sum. Alternately, one can include all products whose weighted periods  $\sum_i (2k_i + 1) T_{\text{PO}_i}$  are less than or equal to a maximum period  $T_{\text{max}}$ . In the present case both prescriptions for truncation are equivalent, because the periods of the orbits are monotonically related to the code lengths. We adopted this truncation scheme and took  $T_{\text{max}}$  to be the period of the orbit coded “+-----”.

The real parts of the zeros of the resulting expansion should correspond to the resonance positions. There are, however, problems, such as the appearance of “false zeros” which clearly are not related to any level in the quantum spectrum. Also, the imaginary parts of the zeros do not agree with the widths of the resonant states. We are, after all, approximating a divergent product. The numerical results are nevertheless quite satisfactory, as shown in Table IX. In the calculation of the triplet energies a phase of  $\pi$  has to be added in (38) for every time the periodic orbit cross the line  $r_1 = r_2$  [18,49]. The energies obtained via cycle expansion, as explained above, are listed in the columns of Table IX labeled “SC1.” Except for the lowest two singlet states, the energies of resonances where both electrons have the same or similar quantum numbers are reproduced with a deviation of ca. 3% or less.

Whether or not a continuation of the cycle expansion to longer code lengths leads to an improvement of the results and eventually to convergence against the exact quantum-mechanical values is not known. In the other direction Wintgen *et al.* [17,18] found that truncating the cycle expansion to only the shortest collinear periodic orbit (code “-”) yields rather accurate results for intrashell resonances of real helium.

When we truncate the expansion of the product (37) after just one term and neglect the instability exponent  $\lambda_{\text{PO}}$ , we obtain the condition

$$S_{\text{PO}} = \frac{S_{\text{PO}}^{(s)}}{\sqrt{-E}} = \left[ n + \frac{\mu_{\text{PO}}}{4} \right] 2\pi\hbar, \quad (39)$$

which is just the conventional formula for semiclassical quantization. The scaling property leads immediately to a Rydberg formula,

$$E_n = - \frac{(S_{\text{PO}}^{(s)})^2}{h^2(n - \mu_s)^2}, \quad (40)$$

as in (14), with a modified Rydberg constant depending on the scaled action of the periodic orbit, and a quantum defect essentially given by the Morse index. The scaled action of the orbit “-” yields a modified Rydberg constant of the right magnitude. For both real helium [17] and  $s$ -wave helium, agreement with the calculated  $NsNs$  levels is good for a quantum defect which is small or almost integer. In the case of  $s$ -wave helium, the Morse index of the orbit “-” is 2 (as in collinear helium), but there is no third dimension and no justification for a winding number contribution, so the quantum defect is close to half-integer. This means that naive WKB-type quantization leads to virtually maximum deviations in the energies of the symmetrically excited states in the

TABLE IX. Semiclassical approximations of binding energies of singlet and triplet states in  $s$ -wave helium calculated with a cycle expansion including periodic orbits up to the weighted period of the “+ - - - -” orbit (i.e., up to code length 6) (SC 1) and with a simpler truncation based on only three nonretracing orbits “+ + - + - -,” “+ + - - + -,” and “+ - + - - -” (SC 2), together with the corresponding values from the quantum-mechanical calculation (QM).

Configuration $^1S_0$	Binding energy (a.u.)			Configuration $^3S_1$	Binding energy (a.u.)		
	SC1	SC2	QM		SC1	SC2	QM
1s1s	2.587	2.872	2.879	1s2s	2.116		2.174
2s2s	0.774	0.722	0.723	2s3s	0.604		0.585
2s3s	0.565		0.572	2s4s	0.526		0.542
3s3s	0.328	0.321	0.321	3s4s	0.278	0.270	0.272
3s4s	0.265	0.260	0.265	3s5s	0.253	0.245	0.251
4s4s	0.180	0.181	0.181	4s5s	0.158	0.158	0.158
4s5s	0.153	0.154	0.154	4s6s	0.146	0.147	0.145
4s6s	0.144	0.143	0.144	5s6s	0.102	0.104	0.103
4s7s	0.136		0.138	5s7s	0.0956	0.0977	0.0954
5s5s	0.114	0.115	0.116				
5s6s	0.100	0.101	0.100				
5s7s	0.0958	0.0954	0.0941				
5s8s	0.0908	0.0899	0.0903				

present case of  $s$ -wave helium. In order to obtain as good agreement as reported for real helium on the basis of the “-” orbit alone [17], we would need an excuse for including a further term  $\frac{1}{2}$  in the quantum defect.

However, an alternate truncation of the cycle expansion does work surprisingly well for  $s$ -wave helium. It is based on the so-called intermittent regions of the potential where the motion is almost integrable. In the classical dynamics of  $s$ -wave helium the equations of motion are separable in the regions  $r_1 > r_2$  and  $r_1 < r_2$ . The coupling of the two degrees of freedom which makes the dynamics chaotic takes place only on the line  $r_1 = r_2$  [24]. So we have large intermittent regions where the motion is not only almost, but exactly integrable. One consequence hereof is the occurrence of infinite sequences of periodic orbits which have a growing part in the intermittent region and whose Lyapunov exponent tends to zero. It has been suggested [58] that these infinite sequences of periodic orbits with diminishing instability have to be considered separately, and that only the remaining periodic orbits should be considered for the cycle expansion.

There are basically two different types of periodic orbits in  $s$ -wave helium. In one type the periodic orbits have two turning points where both electrons simultaneously reverse their direction of motion and then retrace the orbit. The second type consists of those orbits which have no such turning points but close in coordinate space. All orbits of the first type can be grouped in infinite sequences of periodic orbits which have a growing part in an intermittent region by attaching further oscillations to the turning points. This corresponds to an extension of the codes with sequences of “+” signs. The second type of periodic orbits have no such “end” where a “tail” of extra oscillations can be attached, and they are the only periodic orbits which cannot naturally be included in an infinite sequence. We therefore tried a truncation of the cycle expansion using only these second-type orbits, of which there are just 3 up to code length 6 (namely, “+ + - + - -,” “+ + - - + -,” and

“+ - + - - -”; see Fig. 5). The columns labeled “SC2” in Table IX show the results of this quantization. The symmetrically and nearly symmetrically excited states and even the ground state are reproduced surprisingly well and in fact better than in the cycle expansion based on all periodic orbits (up to a given weighted period).

## VI. DISCUSSION AND CONCLUSION

We have presented comprehensive results for the energies of the bound states and energies and widths of autoionizing resonant states in  $s$ -wave helium below the two-electron ionization threshold. The  $1sns$  bound states can be considered as a fair approximation to the corresponding bound states of real three-dimensional helium. In fact, the difference between the  $1sns$  states of  $s$ -wave helium and real helium can be summarized in a small, virtually  $n$ -independent shift  $\Delta\mu$  in the quantum defects, which are slightly smaller in  $s$ -wave helium than in real helium. The difference amounts to  $\Delta\mu = 0.011$  for the singlet states and to  $\Delta\mu = 0.004$  for the triplet states.

All  $Nsns$  states with  $N > 1$  ( $n \geq N$ ) lie above the one-electron ionization threshold and form Rydberg series of autoionizing resonances. The dominant decay mode of these resonances is into the closest open channel, which carries the label  $N - 1$  (for sufficiently large  $n$ ). Perturbation of the Rydberg series  $Nsns$  of resonances by states from the  $N + 1$  channel begin to appear at  $N = 5$  for the singlet states and at  $N = 7$  for the triplet states. The quantum defects of the bound states and resonances in the unperturbed parts of the Rydberg series are well described by an empirical double-Rydberg formula. For each symmetry, singlet or triplet, a four-parameter formula reproduces more than 50 quantum defects within an rms deviation of less than 0.016.

The normalized widths of the autoionizing resonant states increase with channel label  $N$ . The widths of the singlet states begin to become larger than typical separations of successive states in the Rydberg series for  $N = 8$ . At high excitation energies, where the statistical proper-

ties of the spectrum are expected to reflect the chaoticity of the classical dynamics, the quantum spectrum does not consist of many individual lines due to coupling large numbers of Rydberg series as discussed in [59], but rather has the form of a fluctuating continuum due to many overlapping resonances [60] as originally described by Ericson [61].

In the region where a relatively small number of Rydberg series interfere, there are typical perturbation effects which can be described in the framework of multichannel quantum-defect theory. Inhibited autoionization characteristic of a perturbed series of autoionizing resonances is observed, e.g., in the  $7sns$  series, where perturbation due to the  $8s8s$  resonant state leads to a suppression of the total autoionization width by more than three powers of 10.

Semiclassical theories connecting the quantum-mechanical spectrum to the unstable periodic orbits of the corresponding classical system can be applied in the present case. The scaled actions of the shorter periodic orbits show up as peaks in the Fourier-transformed spectrum, as expected on the basis of Gutzwiller's trace formula (36). Attempts to reproduce individual low-lying energy levels by summing the trace formula via the cycle-expansion technique are about as successful as similar applications using collinear orbits to derive semiclassical approximations to the eigenvalues of real helium [18]. Remarkably good results are obtained with a truncation of the cycle expansion based on only three nonretracing periodic orbits.

$s$ -wave helium is a model, and its relation to real helium becomes less clear for higher excitations of both electrons, where angular correlations become increasingly important. However, as a model of two electrons in-

teracting with each other and a nucleus via long-range Coulomb forces, it is perhaps the simplest system still fulfilling this claim. Some of the results of the present investigation may be expected to be relevant for real two-electron atoms, in particular regarding the following points.

(i) The simple unperturbed Rydberg structure of the bound states is virtually the same as in real helium.

(ii) Effects of perturbations as described in multichannel quantum-defect theory will also be seen in real helium. Inhibited autoionization has in fact been observed in a calculation of resonances in real helium by Bürgers and Wintgen [62].

(iii) The fact that the normalized autoionization widths increase towards the two-electron ionization threshold and that the line spectrum becomes a continuum below this threshold may also show up in real helium; in real helium this may be expected to happen at larger excitations, because the diagonalization among the various Rydberg series converging to the same threshold will tend to reduce the effective influence of the electron-electron interaction. In this context, it is interesting to note, that the (lower) quantum number  $N=8$ , where the singlet spectrum of  $s$ -wave helium begins to merge into a continuum, corresponds to the highest doubly excited states of real helium individually observed in the most recent experiments [3].

#### ACKNOWLEDGMENTS

We thank the Deutsche Forschungsgemeinschaft for support. Andre Bürgers and the late Dieter Wintgen kindly supplied results of their studies of three-dimensional helium prior to publication.

- 
- [1] R. P. Madden and K. Codling, *Phys. Rev. Lett.* **10**, 516 (1963).
- [2] J. W. Cooper, U. Fano, and F. Prats, *Phys. Rev. Lett.* **10**, 518 (1963).
- [3] M. Domke *et al.*, *Phys. Rev. Lett.* **66**, 1306 (1991); M. Domke *et al.*, *Verh. Dtsch. Phys. Ges.* (VI) **29**, 396 (1994).
- [4] M. Domke, G. Remmers, and G. Kaindl, *Phys. Rev. Lett.* **69**, 1171 (1992).
- [5] F. H. Read, *J. Phys. B* **10**, 449 (1977).
- [6] F. H. Read, *Aust. J. Phys.* **35**, 475 (1982).
- [7] F. H. Read, *J. Phys. B* **23**, 951 (1990).
- [8] U. Fano, *Rep. Prog. Phys.* **46**, 97 (1983).
- [9] D. R. Herrick, *Adv. Chem. Phys.* **52**, 1 (1983).
- [10] C. D. Lin, *Phys. Rev. A* **29**, 1019 (1984).
- [11] Y. K. Ho, *Phys. Rev. A* **34**, 4402 (1986).
- [12] I. K. Dmitrieva and G. I. Plindov, *J. Phys. B* **22**, 1297 (1989).
- [13] I. K. Dmitrieva, G. I. Plindov, and S. K. Pogrebnya, *J. Phys. B* **25**, 4693 (1992).
- [14] Q. Molina, *Phys. Rev. A* **39**, 3298 (1989).
- [15] K. Richter and D. Wintgen, *Phys. Rev. Lett.* **65**, 1965 (1990).
- [16] J.-M. Rost and J. S. Briggs, *J. Phys. B* **24**, 4293 (1991).
- [17] G. S. Ezra, K. Richter, G. Tanner, and D. Wintgen, *J. Phys. B* **24**, L413 (1991).
- [18] D. Wintgen, K. Richter, and G. Tanner, *Chaos* **2**, 19 (1992).
- [19] K. Richter, Doctoral thesis, Albert-Ludwigs-Universität Freiburg im Breisgau, 1991.
- [20] K. Richter, J. S. Briggs, D. Wintgen, and E. A. Solovev, *J. Phys. B* **25**, 3929 (1992).
- [21] L. Zhang and A. R. P. Rau, *Phys. Rev. A* **46**, 6933 (1992).
- [22] J. Müller, J. Burgdörfer, and D. Noid, *Phys. Rev. A* **45**, 1471 (1992).
- [23] Y. Gu and J.-M. Yuan, *Phys. Rev. A* **47**, R2442 (1993).
- [24] G. Handke, M. Draeger, and H. Friedrich, *Physica A* **197**, 113 (1993).
- [25] G. Handke, M. Draeger, W. Ihra, and H. Friedrich, *Phys. Rev. A* **48**, 3699 (1993).
- [26] G. Handke, Doctoral thesis, Technical University Munich, Verlag Marie L. Leidorf, Buch am Erlbach, 1993.
- [27] R. Poet, *J. Phys. B* **11**, 3081 (1978).
- [28] R. Poet, *J. Phys. B* **13**, 2995 (1980).
- [29] R. Poet, *J. Phys. B* **14**, 91 (1981).
- [30] D. H. Oza and J. Callaway, *Phys. Rev. A* **27**, 2840 (1983).
- [31] B. H. Bransden, R. Hewitt, and H. Plummer, *J. Phys. B* **21**, 2645 (1988).
- [32] A. K. Bhatia, B. I. Schneider, and A. Temkin, *Phys. Rev. Lett.* **70**, 1936 (1993).
- [33] H. Shull and P.-O. Löwdin, *J. Chem. Phys.* **30**, 617 (1959).
- [34] C. Schwartz, *Phys. Rev.* **126**, 1015 (1962).
- [35] N. W. Winter, A. Laferrière, and V. McKoy, *Phys. Rev. A*

- 2, 49 (1970).
- [36] N. W. Winter and V. McKoy, *Phys. Rev. A* **2**, 2219 (1970).
- [37] F. Y. Hajj, *J. Phys. B* **15**, 683 (1982).
- [38] A. Bürgers and D. Wintgen (private communication).
- [39] Y. Accad, C. L. Pekeris, and B. Schiff, *Phys. Rev. A* **4**, 516 (1971).
- [40] S. Saito, *Prog. Theor. Phys.* **40**, 893 (1968).
- [41] S. Saito, S. Okai, R. Tamagaki, and M. Yasumo, *Prog. Theor. Phys.* **50**, 1561 (1973).
- [42] H. Friedrich, *Theoretical Atomic Physics* (Springer-Verlag, New York, 1991).
- [43] A. A. Radzig and B. M. Smirnov, *Reference Data on Atoms, Molecules, and Ions* (Springer-Verlag, New York, 1985).
- [44] H. Friedrich and D. Wintgen, *Phys. Rev. A* **32**, 3231 (1985).
- [45] J. Neukammer *et al.*, *Phys. Rev. Lett.* **55**, 1979 (1985).
- [46] M. Aymar, *J. Phys. B* **18**, L763 (1985).
- [47] A. Giusti-Suzor and H. Lefebvre-Brion, *Phys. Rev. A* **30**, 3057 (1984).
- [48] D. Wintgen and H. Friedrich, *Phys. Rev. A* **35**, 1628 (1987).
- [49] M. C. Gutzwiller, *Chaos in Classical and Quantum Mechanics* (Springer-Verlag, New York, 1990).
- [50] J.-H. Kim and G. S. Ezra, *Proceedings of the Adriatic Conference on Quantum Chaos*, edited by H. A. Cerdeira, R. Ramaswamy, M. C. Gutzwiller, and G. Casati (World Scientific, Singapore, 1991), p. 436.
- [51] See Chaos focus issue on periodic orbit theory, *Chaos* **2**, (1) (1992).
- [52] A. Voros, *J. Phys. A* **21**, 685 (1988).
- [53] P. Cvitanović, *Phys. Rev. Lett.* **61**, 2729 (1988).
- [54] P. Cvitanović and B. Eckhardt, *Phys. Rev. Lett.* **63**, 823 (1989).
- [55] R. Artuso, E. Aurell, and P. Cvitanović, *Nonlinearity* **3**, 325 (1990).
- [56] G. Tanner and D. Wintgen, *Chaos* **2**, 53 (1992).
- [57] F. Christiansen and P. Cvitanović, *Chaos* **2**, 61 (1992).
- [58] P. Dahlgvist, *Chaos* **2**, 43 (1992); *J. Phys. A* **25**, 6265 (1992).
- [59] M. Draeger and H. Friedrich, *Phys. Rev. A* **44**, 3346 (1991).
- [60] T. Ericson and T. Mayer-Kuckuk, *Annu. Rev. Nucl. Sci.* **16**, 183 (1966); R. Blümel and U. Smilansky, *Phys. Rev. Lett.* **60**, 477 (1988); *Physica D* **36**, 111 (1989).
- [61] T. Ericson, *Phys. Rev. Lett.* **5**, 430 (1960).
- [62] A. Bürgers and D. Wintgen, *J. Phys. B* **27**, 131 (1994).